IEEE Access
Multidisciplinary | Rapid Review | Open Access Journal

Received August 2, 2020, accepted August 20, 2020, date of publication August 24, 2020, date of current version September 4, 2020.

Digital Object Identifier 10.1109/ACCESS.2020.3019076

Bandstop Filter Synthesis Scheme for Reactively Loaded Microstrip Line Based 1-D Periodic Structures

IRFAN SHAHID[1], (Student Member, IEEE), DUSHMANTHA N. THALAKOTUNA[2], (Senior Member, IEEE), DEBABRATA K. KARMOKAR[3], (Senior Member, IEEE), AND MICHAEL HEIMLICH[1], (Senior Member, IEEE)

[1]Faculty of Science and Engineering, School of Engineering, Macquarie University, Sydney, NSW 2109, Australia
[2]School of Electrical and Data Engineering, University of Technology Sydney, Ultimo, NSW 2007, Australia
[3]UniSA STEM, University of South Australia, Adelaide, SA 5095, Australia

Corresponding author: Irfan Shahid (irfan.shahid@hdr.mq.edu.au)

This work was supported by the International Macquarie University Research Training Program (iMQRTP).

ABSTRACT A 1-D finite electromagnetic bandgap (EBG) periodic structure is studied. In the structure, EBG behaviour arises from a unit cell comprised of a metallic patch sandwiched between microstrip line and ground plane. Reactive loading offered by patch size determines the bandgap position. A detailed parametric study of various physical structure parameters is presented as a basis to develop a interrelation between physical parameters of the structure and cutoff frequencies. Closed-form synthesis equations are then formulated using curve fitting techniques. Subsequently, a step-by-step design methodology is presented to get a close first pass approximation of structure dimensions for a given specification. This design method reduces the effort required for a designer to perform extensive electromagnetic simulations at early stages of the design. The proposed synthesis method is tested for a variety of commercially available substrates and different frequency ranges for validation. Comparison with electromagnetic (EM) simulations and measurement show that the proposed synthesis method provides first pass approximation of the physical structure dimensions with 94% accuracy.

INDEX TERMS Bandstop filter, electromagnetic bandgap, filter design, microstrip line, periodic structure.

I. INTRODUCTION

Periodic Structures offering EBG characteristics have gained importance in the recent past where they have found applications in various ultra wideband systems [1]. Along with filters and antennas, these structures are also finding their applications in directional couplers, mixers and sensors [2]–[10]. In microstrip line-based periodic structures, EBG characteristics are usually achieved by either regular variation of line width [11], [12], or by loading the line with defected ground structures [12]–[15].

In planar EBG structures, the use of tapered microstrip lines offer steeper roll off rates at the cutoffs with good bandstop rejections, but at the cost of longer structures [11], [39]. Etching patterns in ground plane offers miniaturized structures with the cost of poor roll off factors as in [12], [13], [40], [41]. Furthermore, these DGS structures are difficult to implement in integrated circuits such as MMICs. In 3-D printing, structures with variable substrate thickness also give rise to EBG behavior [16].

EBGs can be created in numerous ways. Periodically loading a transmission line with the help of a shorted patch is another approach [17], [18], [20]–[25]. These structures are realized with three metal layers: a sandwich of a patch (layer 2) between the transmission line (on layer 1) and ground plane (layer 3), as shown in Fig. 1. Reactive loading depends on the electrical size of the patch and its coupling to the other two layers. This determines the cutoff frequencies and bandwidth of the stopband.

The presented structures have very sharp roll off rates at the cutoff frequencies and excellent rejection capabilities in the stopband with a reasonable structure size. Detailed performance comparison, considering both stopband rejection and passband characteristics, of EBG structures with different reactive loading mechanisms is presented in Table 1. Although the considered structure with via holes is more

The associate editor coordinating the review of this manuscript and approving it for publication was Xiu Yin Zhang.

TABLE 1. Performance comparison of EBG structures with different reactive loading configurations.

Ref	Structure	Configuration	Metal Layers	Structure Length (λ_g)	Passband Return Loss # (dB)	Stopband Rejection (dB)	Rolloff Rate (dB/GHz) for f_1	Rolloff Rate (dB/GHz) for f_2
[11]	Planar EBG	Tapered Microstrip Line	2	2.28	20	30	105	102
[12]		Tapered EBG with DGS	2	0.67	13	32	10.9	57.5
[13]		Dumbbell-shaped DGS	2	0.87	5	40	56	20
[39]		Sinusoidal Tapered Microstrip	2	1.69	3	47	87.5	102.9
[40]		Dumbbell-shaped DGS	2	0.52	5	40	150	12.6
[41]		Tapered Dual Plane EBG	2	2.3	8	35	14	12.2
Fig. 12(a)*	Multi-planar EBG	Shorted Patch Structure	3	1.34	3	40	135	78.2
Fig. 17(b)*				1.23	6	35	115	77

* This work

The return loss given here is for the first ripple from the stopband edge.

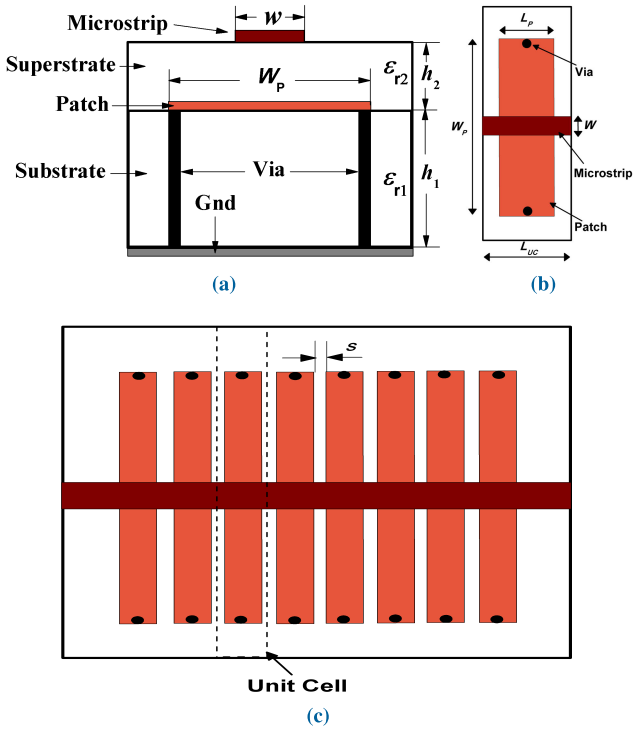

FIGURE 1. (a) Side view and (b) Top view of the Unit Cell. (c) Top view of the periodic structure with 8 unit cells.

costly and complex when compared to the planar structures, the benefits such as steeper roll off rates at both cutoffs, excellent rejections in stopband and compact size make it superior to planar structures. Another advantage of these structures is its suitability for a wide range of two metal layer GaAs and GaN MMIC fabrication processes for implementation of stopband filters in which it is extremely difficult to fabricate DGS.

While there are studies done on analyzing such periodic structures, using circuit models [17]–[19], to determine filter characteristics as a function of physical design parameters. But there has been very limited research on synthesizing a filter using this type of periodic structure to give the reverse: physical design parameters as a function of desired performance. As an example, for a periodic structure, how the unit cell parameters are determined if the specified stopband is defined by given frequencies f_1 and f_2, where, f_1 is the lower cutoff and f_2 is the higher cutoff frequency? A common approach is to start with a known-good design arrived at through the analysis approach. Once the structure is designed and analyzed, its physical structure is resized or modified iteratively and, effectively optimized until desired performance is achieved. Generally, EM simulations for this task could be a time consuming and rigorous exercise. A lumped-circuit equivalent model for such structures aid in mitigating these issues by providing some scalability in ω. However, it is more useful as an analysis tool than a synthesis tool and offers limited help in determining physical structure parameters like widths and lengths etc. to meet a given requirement [17], [18], [26].

A useful approach to design such periodic structures is to have a set of closed form equations to determine cutoff frequencies when parameters such as patch dimensions, substrate thicknesses and dielectric constants are known. A well-known example is the conventional microstrip line impedance and width calculator [27], [28]. Another such example is the design equations being used for calculating the width and length of microstrip patch antennas. These approaches, in general, provide an excellent initial design which performs within a few percent of desired performance. Where more precision is required, a single analysis iteration by slightly adjusting physical parameters, using EM tools, can be used to fine-tune the response to meet the desired specifications.

The baseline EBG structure discussed in this work has been extensively used in literature [17]–[21], [23], [25], [29]–[32]. The unit cell configuration of the structure is slightly changed while maintaining the underlying EBG mechanism to achieve advanced features like dual stopband performance [21], [32], compactness [19], etc. However, the novelty of this study is the development of closed-form equations for baseline rectangular patch structures which are shorted from both ends, not proposing a new structure. In this context, the baseline EBG structure is leveraged to show the efficacy and veracity of the closed-form synthesis equations. This is the first time a concise yet detailed synthesis scheme for the design of this type of periodic structure is proposed that takes filter specifications as input and yields

structure dimensions as a first pass approximation. Unlike previous studies on such structures that use circuit analyses or dispersion analyses to iteratively achieve performance specifications, here, the emphasis is on the formulation of physical design parameters as a function of desired performance. This study will be extremely helpful for the circuit designers in the initial stages of the design and would enable them to numerically calculate physical dimensions of the considered structure using the proposed equations. This will also reduce lots of full-wave simulations using commercial software which requires significant computing resources.

The paper is organized as follows. First, the considered structure is discussed in Section II. Then, a detailed parametric study, along with numerical formula extraction, is presented in Section III. Validation of the proposed closed form equations with the help of numerical simulations and measurements is described in Section IV. Then, these synthesis routines are turned into a step by step procedure to aid the circuit designers in the design process. For verification of the design method, several design examples are presented for various commercially available substrates in Section V followed by concluding remarks in Section VI.

II. STRUCTURE

The periodic structure considered in this work is a three metal layer stack up as shown in Fig. 1. This consists of a substrate with dielectric properties as ε_{r1}, h_1, tanδ and a superstrate with ε_{r2}, h_2, tanδ as shown in Fig. 1. A microstrip line, with 'w' width, is reactively loaded by a metallic patch which is sandwiched between microstrip line and ground plane. The patch is connected to ground through vias placed at both ends. The distance between the adjacant patches is represented by s, as shown in Fig. 1(c). Several such unit cells are placed sequentially such that the structure is sufficiently large enough to give rise to EBG characteristics as a consequence of Bloch periodicity. These structures are capable of producing very sharp roll-off rates as high as 120 dB per octave for transition between passband and stopbands, and vice versa [29]. Furthermore, shorting vias, with radius R_v, can be placed at different positions along the patch [30]–[32]. This alters the current path to ground thereby presenting different effective resonant patch lengths to the microstrip. Moreover, changing via radius R_v alters the inductance thus changing the effective reactive load to the microstrip line. This results in a slight variation in the bandgap edges [32]. In order to reduce the complexity of the equation development process and to capture the reactive loading offered by patch, the radius of vias is maintained fixed and vias are placed at the outer edges of the patch.

Fig. 2(a) presents typical insertion loss performance of the 1-D periodic structure. These structures present very steep roll offs at the band edges. Therefore, it is a common practice to consider operating bandwidth at a reference level of -10 dB or -20 dB [14], [33]–[35]. Here, upper and lower frequency cutoffs at -10 dB reference level are denoted by f_1 and f_2, respectively. Fig. 2(b) shows the sample 1-D

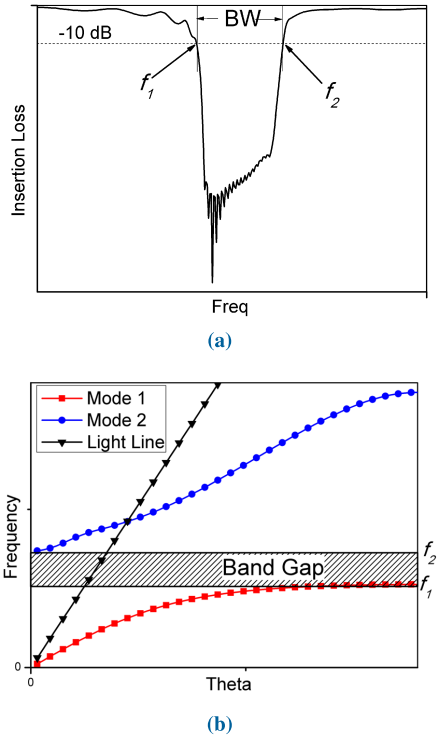

FIGURE 2. (a) Typical S_{21} response of a 1-D periodic structure. (b) Dispersion diagram showing the operating modes and bandgap effect under the light line.

dispersion diagram of the unit cell. This diagram shows the existence of bandgap between the first two modes. The corresponding guided wave band edges under the light line are marked with f_1 and f_2.

III. PARAMETRIC STUDY AND NUMERICAL FORMULA EXTRACTION

In this section, a detailed parametric study is presented to discuss the effect of each structure parameter on the start f_1 and stop f_2 frequencies of the bandgap. S-parameter curves resulting from this parametric study are presented and the -10 dB referenced f_1 and f_2 values are used for determining the effect of each parameter on percentage bandwidth. Baseline parameters used for this study are $\varepsilon_{r1} = \varepsilon_{r2} = 3.0$, $h_1 = 0.75$ mm, $h_2 = 0.16$ mm, $W_P = 8$ mm, $L_P = 2.8$ mm, $s = 1.25$ mm, $w = 1.5$ mm, $R_v = 0.125$ mm and $L_{UC} = 4.05$ mm. It is observed that as the number of unit cells is increased, it results in steeper rolloff rates and higher rejection levels in the stopband without affecting bandgap edges. However, when N is greater than 6, the finite structure exhibits the characteristics similar to a periodic structure with a large number of unit cells. $N = 8$ has been used in our simulations to ensure that the structure is sufficiently large enough to exhibit higher rejections and sharper rolloffs at the cutoffs. All the simulations are performed using CST Microwave Studio.

A. EFFECT OF PATCH DIMENSIONS ON EBG

The metallic patch, once sandwiched between microstrip line and ground plane, presents a distinct reactive load determined

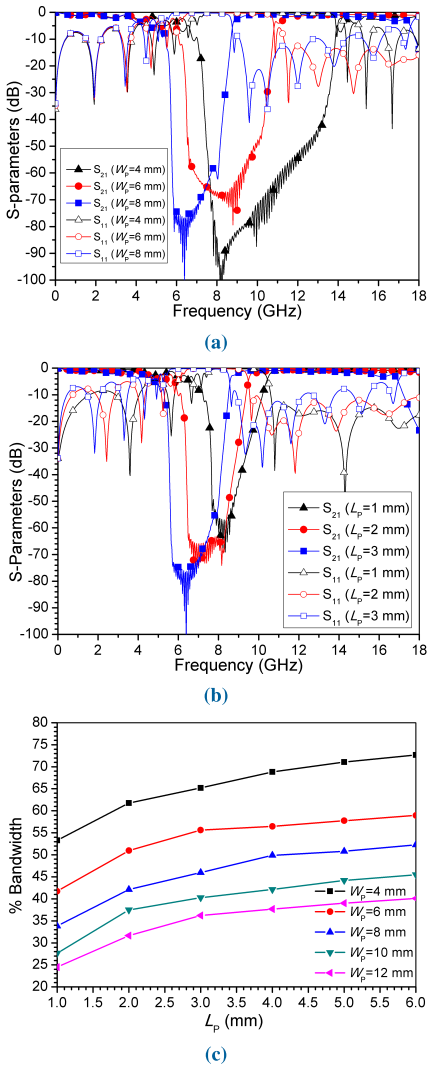

FIGURE 3. S-parameter curves showing the effect on filter bandstop edges by varying (a) W_P when $L_P = 2.8$ mm (b) and varying L_P when $W_P = 8$ mm. (c) Effect on percentage bandwidth for various values of W_P and L_P. The other parameters are fixed as $\varepsilon_{r1} = \varepsilon_{r2} = 3.0$, $h_1 = 0.75$ mm, $h_2 = 0.16$ mm, $s = 1.25$ mm, $w = 1.5$ mm and $L_{UC} = L_P + s$.

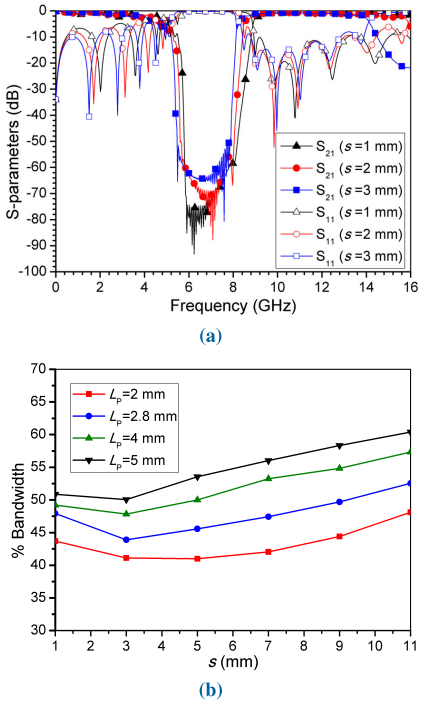

FIGURE 4. (a) S-parameter curves showing the effect on filter bandstop edges by varying s when $L_P = 2.8$ mm. (b) Effect on percentage bandwidth for various values of L_P and s. The other parameters are fixed as $\varepsilon_{r1} = \varepsilon_{r2} = 3.0$, $h_1 = 0.75$ mm, $h_2 = 0.16$ mm, $W_P = 8$ mm, $w = 1.5$ mm and $L_{UC} = L_P + s$.

by the patch dimensions ($W_P \times L_P$). Conceptually, greater values of W_P present longer paths for the induced current (from microstrip) to reach ground, thus causing a reduction in frequency. Different values of W_P while keeping all other factors constant, are simulated and it is observed that increasing patch dimensions causes f_1 and f_2 to scale down as shown in Fig. 3(a). Similarly, increasing L_P induces a larger microstrip-patch interaction causing wider bandgaps at lower frequencies at the cost of poor insertion loss performance in passbands as depicted in Fig. 3(b).

In practical scenarios, care shall be given while choosing the values for L_P as bigger values of L_P increases the size of the filter by a multiple of N. The effect of patch area on the percentage bandwidth is presented in Fig. 3(c) which shows that smaller W_P yields wider percentage bandwidth, whereas, smaller L_P results in narrow bandwidth. So, wider bandwidths from the structure can be achieved with a combination of smaller W_P and larger L_P at the cost of longer filter and poor insertion loss in passband. Percentage bandwidth is calculated as the ratio of the bandwidth to the center frequency as $\frac{BW}{fc} \times 100$. It can also be inferred that f_1 and f_2 are inversely proportional to the patch dimensions and can be expressed as follows:

$$f_1, f_2 \propto \frac{1}{W_P}, \frac{1}{L_P} \tag{1}$$

$$\%BW \propto \frac{1}{W_P}, L_P \tag{2}$$

B. EFFECT OF UNIT CELL LENGTH ON EBG

In a unit cell, L_{UC} is determined by the sum of L_P and spacing s in between. As discussed earlier, increasing L_P causes both cutoff frequencies to shift down with increased percentage bandwidths. Increasing the spacing between patches increases the unit cell dimensions resulting in slightly scaled down frequency cutoffs as shown in Fig. 4(a). A secondary effect of increased spacing is better impedance match in the passbands thereby yielding less passband ripple. Fig. 4(b) presents the impact of spacing on the percentage bandwidth of the filter with various values of L_P. It is observed that when the values of s are comparable to L_P, percentage bandwidth remains unchanged. But when s becomes greater than L_P, bandwidth starts to increase. The dependence of L_P and s on cutoff frequencies and the percentage bandwidth is given as:

$$f_1, f_2 \propto \frac{1}{L_P}, \frac{1}{s} \tag{3}$$

$$\%BW \propto L_P, s \tag{4}$$

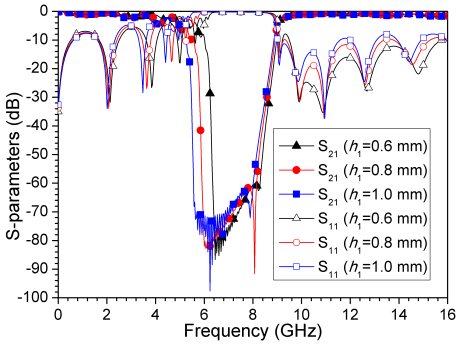

(a)

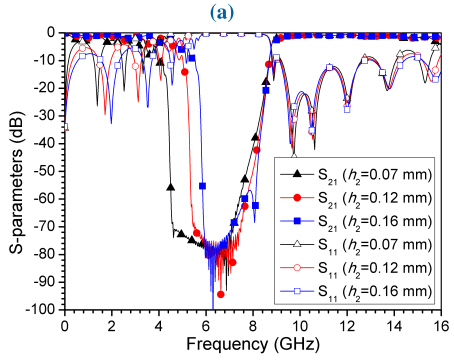

(b)

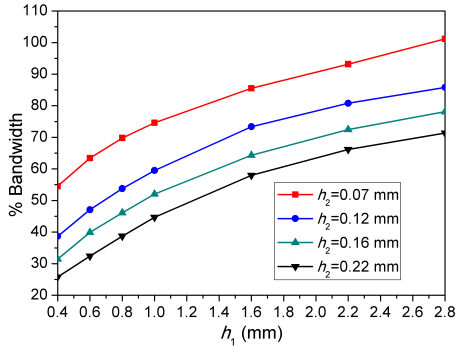

(c)

FIGURE 5. S-parameter curves showing the effect on filter bandstop edges by varying (a) h_1 when $h_2 = 0.16$ mm and (b) by varying h_2 when $h_1 = 0.75$ mm. (c) Effect on percentage bandwidth for various values of h_1 and h_2. The other parameters are fixed as $\varepsilon_{r1} = \varepsilon_{r2} = 3.0$, $W_P = 8$ mm, $L_P = 2.8$ mm, $s = 1.25$ mm, $w = 1.5$ mm and $L_{UC} = L_P + s$.

C. EFFECT OF SUBSTRATE AND SUPERSTRATE HEIGHTS ON EBG

The substrate and superstrate heights are also discussed for their effect on structure performance. Increasing h_2 increases the distance between patch and the microstrip line, resulting in weaker coupling between the two and decreasing the percentage bandwidth of the stopband. Decreasing this distance results in strong coupling which decreases the lower stopband frequency and presents stronger ripples in the passband as shown in Fig. 5(b). So choosing values for h_2 presents a trade-off between the desired bandwidth and the ripples in the passband.

It is observed that increasing h_1 causes f_1 and f_2 to scale down where f_1 is more sensitive to this change as shown in Fig. 5(a). Although, in this figure f_2 does not seem to be affected much by this change. It will be shown in subsequent sections that higher values of h_1 exhibit larger reductions in f_2, as shown in Fig. 5(a). The effect of varying h_1 and h_2 on percentage bandwidth is illustrated in Fig. 5(c), which shows that increasing h_1 causes percentage bandwidth to increase whereas increasing h_2 causes percentage bandwidth to decrease. The cutoff frequencies f_1, f_2 and percentage bandwidth relates to h_1 and h_2 as follows, when all other parameters are constant.

$$f_1 \propto \frac{1}{h_1}, h_2 \tag{5}$$

$$f_2 \propto \frac{1}{h_1} \tag{6}$$

$$\%BW \propto h_1, \frac{1}{h_2} \tag{7}$$

D. EFFECT OF SUBSTRATE AND SUPERSTRATE DIELECTRIC CONSTANTS ON EBG

Changing ε_{r1} has a moderate effect on f_1 and major effect on f_2 as shown in Fig. 6(a). Increasing ε_{r1} causes the band edges to shift down with its smaller values yielding relatively larger bandwidths (Fig. 6(c)). Similarly, increasing ε_{r2} reduces f_1 without affecting f_2 which causes center frequency to shift down with increased percentage bandwidths as shown in Fig. 6(b). It is also observed that higher values of ε_{r2} cause ripples in the passband because of the patch perturbing the wave propagation. Fairly wide stop bandwidths may be obtained by using lower values of ε_{r1} and higher values of ε_{r2} at the cost of passband ripples. A secondary effect of lower ε_{r1} is a larger structure to achieve comparable stopbands. From the discussion and simulation results shown in Fig. 6, it is inferred that f_1 is inversely proportional to ε_{r1} and ε_{r2}, and f_2 has inverse proportion with ε_{r1}. Whereas percentage bandwidth is directly proportional to ε_{r2} and inversely proportional to ε_{r1}. These can be represented as:

$$f_1 \propto \frac{1}{\varepsilon_{r1}}, \frac{1}{\varepsilon_{r2}} \tag{8}$$

$$f_2 \propto \frac{1}{\varepsilon_{r1}} \tag{9}$$

$$\%BW \propto \frac{1}{\varepsilon_{r1}}, \varepsilon_{r2} \tag{10}$$

E. SUMMARY: PRELIMINARY SYNTHESIS FORMULATION

Using (1), (3), 5 and (8), f_1 is a function of all the considered parameters where, W_P, L_P, h_1, h_2, ε_{r2} being major contributors and, s and ε_{r1} being minor contributors. All parameters have an inverse relationship with f_1 except h_2 which is directly proportional to f_1. So f_1 can be expressed as

$$f_1 \propto \frac{1}{W_P}, \frac{1}{L_P}, \frac{1}{s}, \frac{1}{h_1}, h_2, \frac{1}{\varepsilon_{r1}}, \frac{1}{\varepsilon_{r2}} \tag{11}$$

Similiarly, from (1), (3), (6) and (9), f_2 is an inverse function of all parametrs except h_2. In determining the upper frequency cutoff, W_P, L_P and ε_{r1} has got more weightage than s and h_1. So f_2 can be referred to as

$$f_2 \propto \frac{1}{W_P}, \frac{1}{L_P}, \frac{1}{s}, \frac{1}{h_1}, \frac{1}{\varepsilon_{r1}} \tag{12}$$

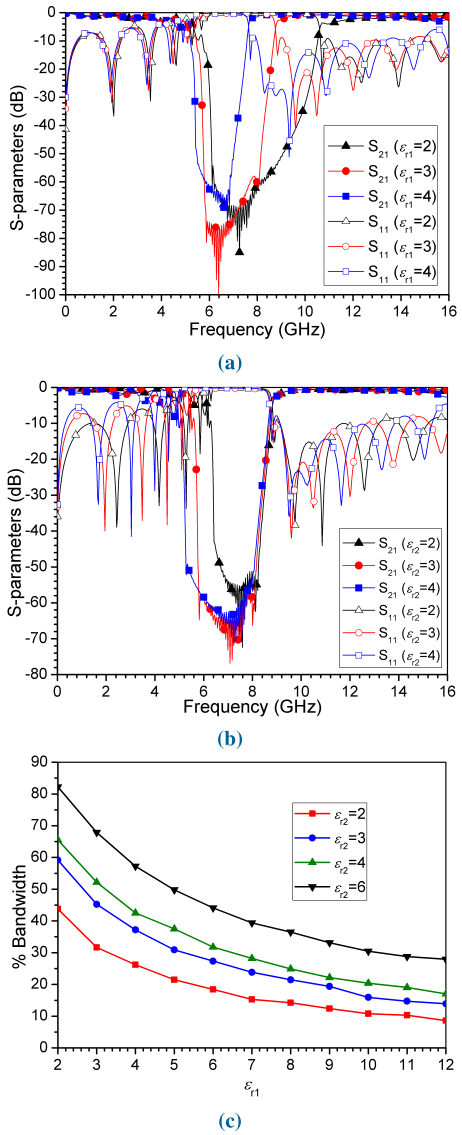

FIGURE 6. S-parameter curves showing the effect on filter bandstop edges by varying (a) ε_{r1} when $\varepsilon_{r2} = 3.0$ and (b) by varying ε_{r2} when $\varepsilon_{r1} = 3.0$. (c) Effect on percentage bandwidth for various values of ε_{r1} and ε_{r2}. The other parameters are fixed as $h_1 = 0.75$ mm, $h_2 = 0.16$ mm, $W_P = 8$ mm, $L_P = 2.8$ mm, $s = 1.25$ mm, $w = 1.5$ mm and $L_{UC} = L_P + s$.

For percentage bandwidth being offered by this structure, (2), (4), (7) and (10) are summarized in (13).

$$\%BW \propto \frac{1}{W_P}, L_P, s, h_1, \frac{1}{h_2}, \frac{1}{\varepsilon_{r1}}, \varepsilon_{r2} \tag{13}$$

In order to represent the cutoff frequencies in terms of structure physical parameters, following step by step procedure was adopted.

1) As a starting point, a basic frequency wavelength relationship, $f = c/(\sqrt{\varepsilon_{re}}\lambda_0)$, was used. Here, the term in denominator accounts for the guided wavelength of the quasi-TEM mode of the microstrip line. For numerically calculating frequency cutoffs, structure parameters such as W_P, L_P and s were represented in terms of wavelength. Whereas, material characteristics and dimensions such as ε_{r1}, ε_{r2}, h_1 and h_2 were used in the calculation of effective dielectric constant, ε_{re}, of the three metal stack-up in the presence of the metallic patch.
2) By using (11) and (12), initial curve fitting was performed to find the dependence of structure parameters on frequency cutoffs while keeping the substrate parameters fixed. Wide range of structure parameter values, with EM simulated frequency cutoffs, were used as a reference to match the result of curve fitting. Various combinations of algebraic operations were iteratively tested on structure parameters to satisfy their contribution/weight in determining the approximate values of frequency band edges.
3) After finding approximate algebraic operation for structure parameters, the same exercise was repeated for substrate parameters where 72 different substrate parameter combinations were used as a reference.
4) Finally, coefficients for each of the structure parameters were iteratively adjusted to match the EM simulation data.

Resultantly, f_1 and f_2 can be approximated using the closed form equations (14) and (15), respectively, in terms of the unit cell parameters as given below:

$$f_1 \approx \frac{1.96c}{\sqrt{\varepsilon_{r1} + 2\varepsilon_{r2}}(1 + 0.6\sqrt{\frac{h_1}{h_2}})(W_P + 2.4L_P + 0.64s)} \tag{14}$$

$$f_2 \approx \frac{0.8c(1 - 0.05\sqrt{h_1})}{(1 + 0.15\sqrt{s})\sqrt{\varepsilon_{r1}}W_P(W_P + 4.7L_P)} \tag{15}$$

where c is the speed of light in m/s, frequency in GHz and all length dimensions are in mm. The proposed set of equations are targeted for EBG filter synthesis for implementation on printed circuit board (PCB) and MMIC technologies above 1 GHz.

IV. VALIDATION OF PROPOSED CLOSED FORM EQUATIONS

Validation of these proposed equations is carried out in two steps. First, different combinations of physical structure parameter values are used to numerically calculate the frequency cutoffs using the proposed closed-form equations. These are compared with the corresponding EM simulated results as a self-consistency validation step. This is carried out to mainly determine how well these equations represent the EM simulated results. Second, a prototype is fabricated and measured for a similar set of substrate parameters to ascertain the validity of EM simulations. This second validation is a more practical verification.

A. VALIDATION OF EQUATIONS

In this step, in order to ascertain the validity of the proposed closed form equations, f_1 and f_2 are calculated for a wide range of the structure physical parameter values and are plotted against corresponding values obtained from EM simulations. Another aim of this detailed parametric study is to find out whether these formulas have fully captured the

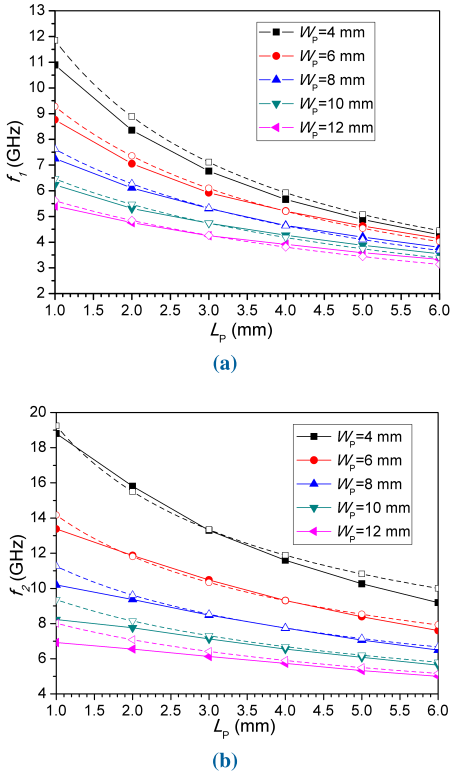

FIGURE 7. Numerical (dashed line) vs EM simulated (continuous line) results showing the effect of W_P and L_P on (a) f_1 and (b) f_2. ($\varepsilon_{r1} = \varepsilon_{r2} = 3.0$, $h_1 = 0.75$ mm, $h_2 = 0.16$ mm, $s = 1.25$ mm and $w = 1.5$ mm).

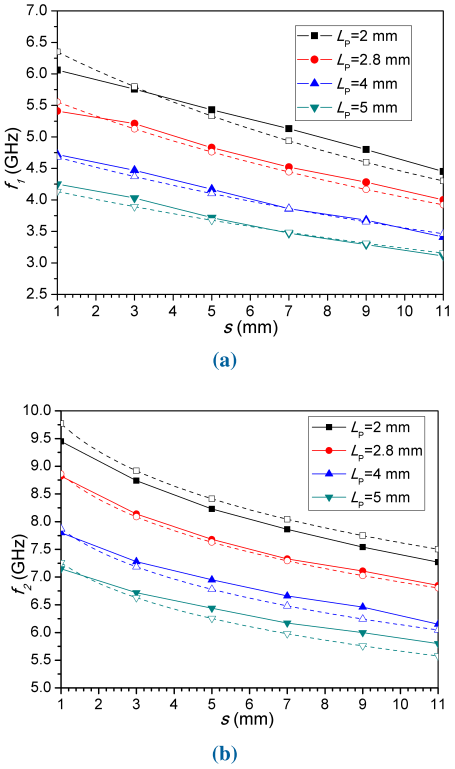

FIGURE 8. Numerical (dashed line) vs EM simulated (continuous line) results showing the effect of L_P and s on (a) f_1 and (b) f_2. ($\varepsilon_{r1} = \varepsilon_{r2} = 3.0$, $W_P = 8$ mm, $h_1 = 0.75$ mm, $h_2 = 0.16$ mm and $w = 1.5$ mm).

behavior of each parameter and can follow the trends for the changing values. Efforts are made to test the proposed formulas for a wide range of structure parameters and find out the limits in which the closed form formulas fully satisfy the EM simulation results. This validation is further carried out in two steps. In first step, substrate parameters are fixed and unit cell dimensions are varied in the shape of patch width, length and gap in between patches. In the second step, unit cell parameters are fixed and substrate parameters are varied in the shape of substrate dielectric constants and heights. In what follows, numerically calculated frequency cutoffs are shown with dotted lines whereas those obtained from EM simulations are in solid lines. Baseline parameters used for this study are $\varepsilon_{r1} = \varepsilon_{r2} = 3.0$, $h_1 = 0.75$ mm, $h_2 = 0.16$ mm, $W_P = 8$ mm, $L_P = 2.8$ mm, $s = 1.25$ mm, $w = 1.5$ mm and $L_{UC} = 4.05$ mm.

1) PATCH AND UNIT CELL DIMENSIONS

Frequency cutoffs resulting from a wide range of patch dimensions have been numerically calculated and EM simulated, and results are shown in Fig. 7. For numerical calculations, each W_P value from a set of 4, 6, 8, 10 and 12 mm is varied against L_P values of 1 to 6 mm with a step size of 0.1 mm. As EM simulations are a time consuming task so each W_P value is simulated against a reduced number of L_P values that is to say from 1 to 6 mm with a step size of 1 mm. It is observed that for larger patch dimensions, the proposed equations are able to predict the cutoff frequencies and are also able to follow the trend for changing the parameter values. However, for smaller patch dimensions comparable to the microstrip width, results slightly deviate from each other with the worst case error being 8.5% for f_1 and 12.7% for f_2.

As discussed earlier, the length of unit cell is sum of the patch length (L_P) along the microstrip line and gap s between two consecutive patches. Therefore, each value of L_P from a set of (2, 2.8, 4 and 5 mm) is simulated against different values of s. Corresponding frequency cutoffs are also numerically calculated and results are presented in Fig. 8. It is observed that proposed formulas are able to capture the trends for changing values of L_P and s.

2) SUBSTRATE PARAMETERS

In order to ascertain the validity of proposed set of equations for different set of substrates, two sets of studies are conducted. Firstly, keeping the patch dimensions ($W_P \times L_P$), unit cell length (L_{UC}), h_1 and h_2 fixed, different values of substrate and superstrate dielectric constants are EM simulated and numerically evaluated. Secondly, patch dimensions, ε_{r1} and ε_{r2} are maintained fixed and h_1 is varied against h_2. Cutoff frequencies are presented in Figs. 9 and 10. It is observed that the results obtained using the proposed equations agrees well with the results from EM simulations. Moreover, the agreement is for a wide range of dielectric constants, e.g., ε_{r1} from 2 to 12 and ε_{r2} from 2 to 6, with the worst-case errors being 2.94% and 2.75% for f_1 and f_2, respectively. This makes the equations suitable for the majority of 2-layer MMIC processes which has average dielectric constants for

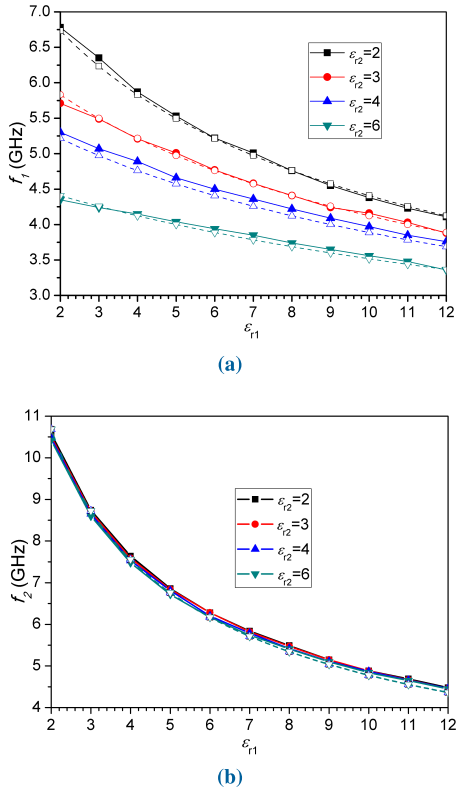

FIGURE 9. Numerical (dashed line) vs EM simulated (continuous line) results showing the effect of ε_{r1} and ε_{r2} on (a) f_1 and (b) f_2. ($h_1 = 0.75$ mm, $h_2 = 0.16$ mm, $W_P = 8$ mm, $L_P = 2.8$ mm, $s = 1.25$ mm and $w = 1.5$ mm).

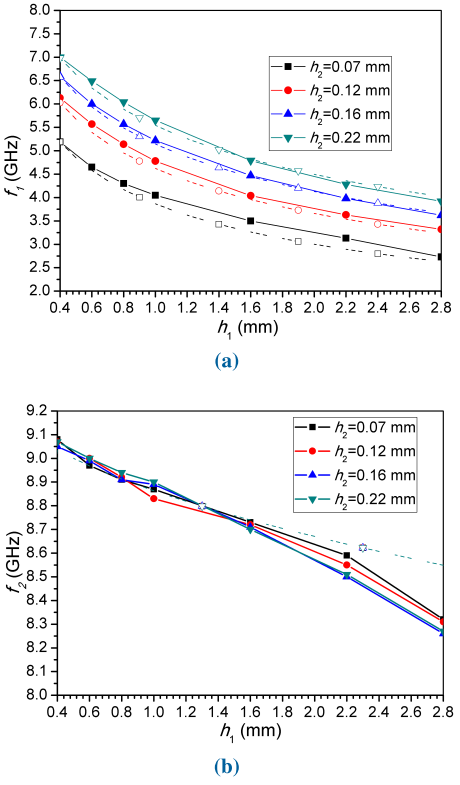

FIGURE 10. Numerical (dashed line) vs EM simulated (continuous line) results showing the effect of h_1 and h_2 on (a) f_1 and (b) f_2. ($\varepsilon_{r1} = \varepsilon_{r2} = 3.0$, $W_P = 8$ mm, $L_P = 2.8$ mm, $s = 1.25$ mm and $w = 1.5$ mm).

ε_{r1} and ε_{r2} as 12.9 and 6.5 respectively. Similarly, Fig. 10 shows that the proposed formulas hold for a wide range of h_2/h_1 as 0.025 to 0.55 resulting from 0.07/2.8 and 0.22/0.4, respectively. Within this range, the maximum error for lower and upper cutoff is 7.9% and 3.4%, respectively. This also shows the suitability of proposed equations for 2-layer MMIC processes which has corresponding h_2/h_1 ratios of 0.02 resulting from 2 microns and 100 microns respective dielectric thicknesses.

B. FABRICATION AND MEASUREMENTS

In order to verify the validity of the EM simulation and numerical results, a test structure is fabricated and measured. For fabrication purposes, substrate and superstrate parameters are kept fixed and multiple boards with different patch parameter combinations are fabricated. Physical patch dimensions are chosen and frequency cutoffs are numerically calculated using the proposed equations (14) and (15), and compared with simulated and measured results. This test structure is fabricated using Rogers RO3003 substrate with $\varepsilon_{r1} = 3.0$, $h_1 = 0.76$ mm and tanδ = 0.001 and Astra MT-77 superstrate with $\varepsilon_{r2} = 3.0$, $h_2 = 0.127$ mm and tanδ = 0.017. Then, these two boards one with patch and ground (substrate) and other with microstrip line on top (superstrate) are joined together with a prepreg sheet of Astra MT-77 of the same dielectric material with thickness of 0.0625 mm. Total thickness of the superstrate including

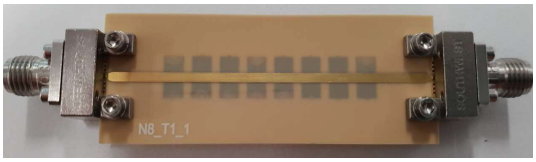

FIGURE 11. Fabricated filter with $W_P = 6.5$ mm, $L_P = 3$ mm, $s = 1.25$ mm, $R_v = 0.125$ mm and $w = 1.5$ mm.

Astra MT-77 core and prepreg is 0.1905 mm. Other parameters are $W_P = 6.5$ mm, $L_P = 3$ mm, $s = 1.25$ mm, $R_v = 0.125$ mm and $w = 1.5$ mm. An additional feed line length of 4.3 mm was added on both sides of the fabricated structures for connecting the end launch SMA connectors to cater for mounting screws. The fabricated filter structure is shown in Fig. 11. Two other filter structures with different basic patch parameters such as W_P and L_P with different values are also presented with EM simulated and numerically calculated cutoffs. In these structures, W_P and L_P are chosen as 8 and 2.8 mm, and, 10 and 4.5 mm, respectively.

Fig. 12(a) shows the s-parameters response of the fabricated filter structure, whereas, Figs. 12(b) and (c) shows the simulated performance compared with the numerical results. The measured results and simulated results are in good agreement. It can be seen that fabricated filter present undesirable increasing pass band ripples around the band edges which is inherited characteristics of the EBG structures [17], [26], [29], [37]. This is due to the mismatch created by the Bloch impedances. Based on the detailed

TABLE 2. Comparison of the −10 dB cutoff frequencies obtained through EM simulation, numerical calculations and measurements.

Filter Structure	W_P	L_P	f_1 (GHz)				f_2 (GHz)			
	(mm)	(mm)	Sim	Calc	Meas	% Error	Sim	Calc	Meas	% Error
1	6.5	3	6.16	6.17	6.26	1.45	10.28	9.81	10.38	5.8
2	8	2.8	5.77	5.76	-	0.17	8.87	8.72	-	1.7
3	10	4.5	4.3	4.14	-	3.8	6.42	6.43	-	0.2

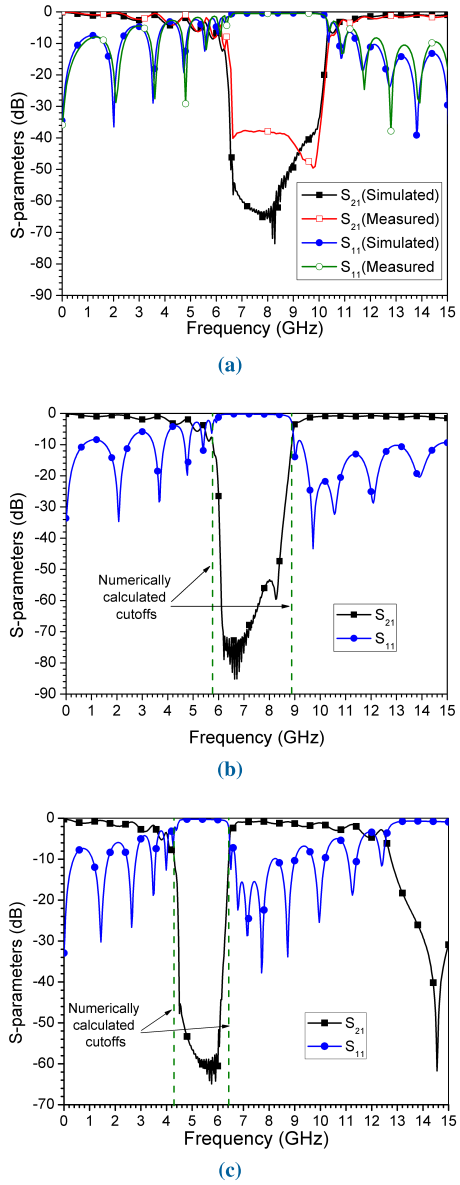

FIGURE 12. (a) Simulated vs measured results for filter structure with patch dimensions as $W_P = 6.5$ mm and $L_P = 3$ mm. Simulated performance for filter structures with (b) $W_P = 8$ mm and $L_P = 2.8$ mm, and (c) $W_P = 10$ mm and $L_P = 4.5$ mm.

parametric study, it is recommended that lower passband ripples can be achieved by using smaller L_P, larger s and thicker superstrates h_2. For the width of microstrip line, as discussed earlier, reactively loading a line decreases its characteristic impedance so using a higher impedance line is recommended. Therefore, we suggest using a microstrip line width corresponding to 50 to 70 Ω impedance so that the insertion loss is acceptable.

A comparison amongst the −10 dB cutoffs obtained through numerical calculations, EM simulations and measurements are summarized in Table 2 for different test structures. Absolute percentage error values are calculated amongst the three categories and the worst values are reported. It is evident from the tabulated values, that the maximum percentage errors amongst the three values are 3.8% for f_1 and 5.8% for f_2. The difference between the predicted and simulated/measured performances is attributed to the assumptions that were made during the equation development process. These are mainly due to the effect of via position and radius, metal layer thicknesses and material losses. It is found that, the proposed set of equations can predict the frequency cutoffs up to an accuracy of 94.2%. This suggests that the proposed set of closed form equations closely estimate the EM simulated data and the measured data. Hence, proposed numerical formulas can be utilized for synthesis. This would greatly reduce design optimization time in comparison to extensive EM simulations.

V. SYNTHESIS PROCEDURE AND DESIGN EXAMPLES FOR VARIOUS SUBSTRATE SETS

The results of Section IV validate the closed-form synthesis equations for a useful range of frequencies and bandwidths on generally available manufacturing technologies. As these formulas can predict the frequency cutoffs up to an accuracy of 94%, they can be used to estimate the structure dimensions for a given set of substrate parameters. This would not only save extensive EM simulation time and effort but also help circuit designers to quickly make a first pass approximation. Then fine tuning can be done with the help of any EM simulator to meet the desired specifications of the bandstop filter. Given the desired specifications for a bandstop filter for a certain frequency band with size constraints, the proposed method can assist the circuit designers with a quick estimate of the structure physical parameters. The synthesis starts with the unit cell design where structure dimensions are calculated using proposed closed-form equations (14) and (15) for required cutoff frequencies. Passband response is controlled by the patch-microstrip overlap at the cost of required stop bandwidth. We recommend measures to limit the passband ripples by use of smaller L_P, larger s and thicker h_2 as discussed in the previous section. Then the finite filter is constructed by cascading at least six unit cells to achieve at least 30 dB rejection in the stopband and steeper roll off rates. Important structure parameters required to make a bandstop filter have been discussed in section II. The proposed synthesis methodology for the design of a reactively loaded microstrip line comprises of the following steps:

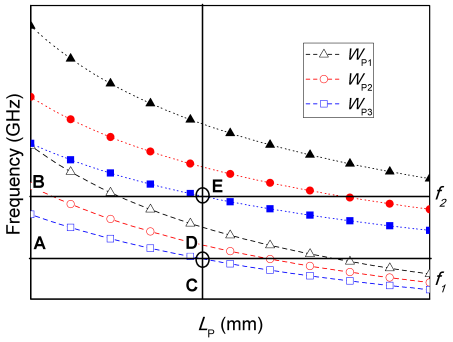

FIGURE 13. f_1 (empty symbols) and f_2 (filled symbols) for different values of W_P and L_P to find out intersection points '*D*' and '*E*' for lines '*A*', '*B*' and '*C*'.

1) Choosing suitable substrate parameters - including dielectric constants and heights. The detailed parametric study presented in Sections III and IV gives an insight about the pros and cons of the effect of different substrate parameters on the frequency cutoffs, percentage bandwidth (13) and passband ripples. Based on these parameters, the width of the microstrip line needs to be calculated which should be at least 50 Ω. Conventional microstrip formulas for multiple stacked substrates can be used to calculate the corresponding width. Higher values of characteristics impedance are recommended as the presence of reactive loads tend to decrease the input/output impedances seen from each port.
2) Unit cell spacing s is critical as it has direct impact on the length of the filter. As discussed earlier, s controls the passband ripples.

$$L_{\text{filter}} = NL_{\text{UC}} = N(L_P + s) \tag{16}$$

where N is the number of unit cells. For values of N greater than 6, the structure is sufficiently large enough to exhibit EBG characteristics [21]. This would produce rejections of the order of 30 dBs in the stopband with sharper roll off rates. However, it presents a trade-off among the available space and required rejection levels across the band alongwith roll off rates at band edges.
3) Patch dimension initial calculation. In this step, f_1 and f_2 are numerically calculated for different values of W_P and L_P using (14) and (15). These frequency cutoffs should be plotted on a single graph with frequency on Y-axis and L_P on X-axis showing responses for varying values of W_P as shown in Fig. 13. Then horizontal lines '*A*' (for lower cutoff) and '*B*' (for upper cutoff) corresponding to the required frequency cutoffs are drawn on the graph. With the help of a constant L_P vertical line '*C*', points '*D*' and '*E*' are marked for a W_P curve that intersects '*A*' and '*B*' line with '*C*'. This would provide the approximate values for W_P and L_P.
4) Initial physical parameter determination. If intersection of lines '*A*', '*B*' and '*C*' is not found and it falls outside the calculated values, then either of the following two steps may be taken. Expand the range of values for W_P and L_P to find out curves for frequency cutoffs and repeat step 3 or choose a different value of gap s and repeat step 3.
5) Initial correction for non-convergence. If step 4 doesn't provide an estimate for the W_P and L_P values, then choose a different substrate parameters and repeat step 2. In some cases, EBG behavior will not be possible because the physical system will not create imaginary propagation constants consistent with emergence of EBG behavior [36].
6) Validation prior to manufacturing. After choosing correct values of W_P and L_P, setup model in an EM simulator and perform fine tuning to achieve the required frequency cutoffs.

In the upcoming paragraphs, verification of the proposed design scheme would be presented with the help of few design examples for different set of commercially available substrates and varying frequency requirements.

A. DESIGN EXAMPLE 1 (FOR ROGERS DUROID RO3003 MATERIAL)

A filter is designed for a stop band frequency range of 8 to 12 GHz. For this filter, commonly available substrate and superstrate dielectric constants $\varepsilon_{r1}, \varepsilon_{r2} = 3$ with corresponding thicknesses of $h_1 = 0.75$ mm, $h_2 = 0.19$ mm are used. As described in the design procedure width of the microstrip line is chosen as $w = 1.5$ mm which corresponds to a characteristic impedance of 65 Ω. Gap 's' between the patches is chosen as 1.5 mm and cutoff frequencies are plotted for different values of L_P and W_P using (14) and (15) as shown in Fig. 14(a). Then, intersection of horizontal lines '*A*' and '*B*' with vertical line '*C*' is marked as '*D*' and '*E*', respectively. This yields the values of L_P as 1.5 mm and W_P as 6.5 mm labelled as option-1 in Fig. 14(a). Other combinations of L_P and W_P may also be possible such as $L_P = 1.9$ mm and $W_P = 6$ mm (option-2) which would also provide approximated structure values but it would require more tuning. Both these options are EM simulated in CST and corresponding s-parameter plots are presented in Fig. 14(b). As the structure dimensions obtained through option-1 represent the closest approximation, it yields the required frequency cutoffs and in this case it doesn't require tuning. For option-2, it provides a rough estimate of the structure dimensions but because the intersection points don't lie on the vertical line '*C*', therefore, it would require additional tuning using EM simulations.

B. DESIGN EXAMPLE 2 (FOR TACONIC RF-35 MATERIAL)

In the second design example, a bandstop filter is designed for a frequency range of 12 to 18 GHz. For this example, substrate and superstrate are chosen as Taconic RF-35 material with dielectric constant of 3.55. Substrate and superstrate thicknesses are chosen as 0.508 and 0.2 mm, respectively, with a corresponding microstrip width of 1.35 mm. Then gap 's' is fixed as 1 mm and different patch dimensions are used to estimate the frequency cutoffs using (14) and (15) as shown in Fig. 15(a). Then, intersections are marked for line

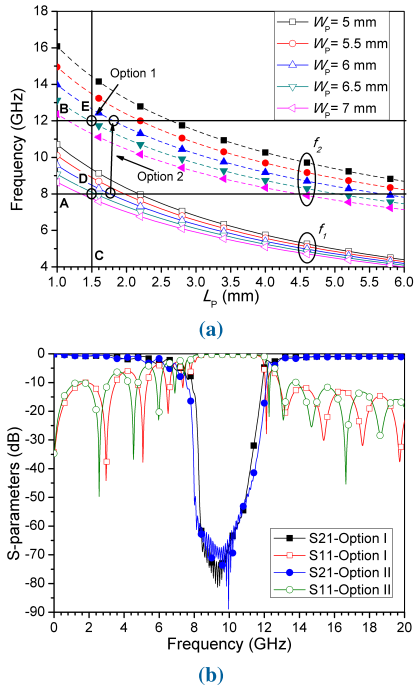

FIGURE 14. (a) Frequency cutoffs plotted for different values of W_P and L_P calculated using (14) and (15). (b) S-parameter response of the filter using the structure physical parameters determined from intersections of line '*A*' and '*B*' with vertical line '*C*' as option-I and 2nd best intersection as option-II.

'*A*' and '*B*' with line '*C*'. As there is no intersection point '*D*' and '*E*' available for a vertical line '*C*', therefore, a much fine tuning sweeps for W_P values would be required. But to show the rigidity of the proposed method, approximated values of $W_P = 3.5$ mm and $L_P = 1.5$ mm are used as structure parameters. Fig. 15(b) presents the corresponding s-parameter plot for the determined structure dimensions. It is noted that the structure physical parameters determined using the proposed synthesis method meets the lower frequency cutoff and slightly off for the upper frequency cutoff and needs tuning.

C. DESIGN EXAMPLE 3 (FOR ROGERS DUROID RO5880 AND RO6006 MATERIALS)

In order to show the validity of the proposed method for a wider frequency range and substrate set, third design example is chosen for the design of a filter for a frequency range of 6 to 12 GHz. For the implementation of this filter, substrate and superstrate are chosen as Rogers Duroid RO5880 and RO6006 with $\varepsilon_{r1} = 2.2$ with $h_1 = 0.5$ mm and $\varepsilon_{r2} = 6.15$ with $h_2 = 0.2$ mm, respectively. Width of microstrip line is chosen as 1.35 mm and gap 's' as 1 mm. Fig. 16(a) shows the frequency cutoffs numerically calculated for different values of L_P and W_P. Then intersection points '*D*' and '*E*' are marked for lines '*A*' and '*B*' with line '*C*' which yields patch dimensions as $W_P = 7.5$ mm and $L_P = 2.1$ mm. Fig. 16(b) shows the s-parameter response for the determined physical structure parameters. It can be seen that even without any need to tune using EM simulations, the proposed method is able to correctly predict the frequency cutoffs.

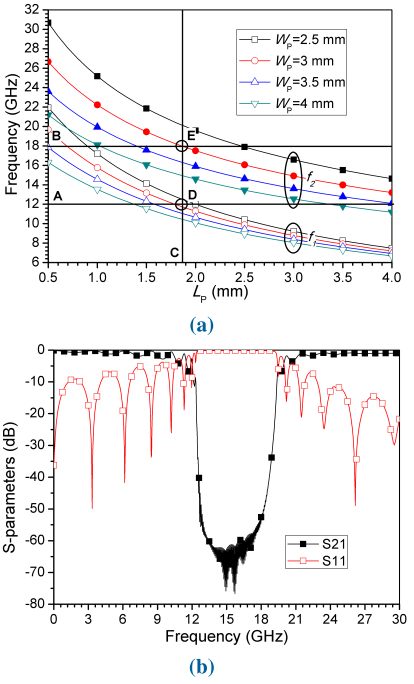

FIGURE 15. (a) Frequency cutoffs plotted for different values of W_P and L_P calculated using (14) and (15). (b) S-parameter response of the filter using the structure physical parameters determined using proposed synthesis method.

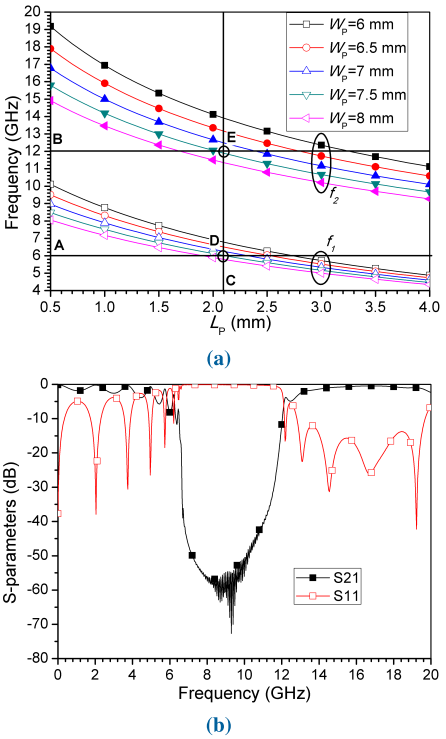

FIGURE 16. (a) Frequency cutoffs plotted for different values of W_P and L_P calculated using (14) and (15). (b) S-parameter response of the filter using the structure physical parameters determined using proposed synthesis method.

D. DESIGN EXAMPLE 4 (Improved RETURN LOSS PERFORMANCE IN THE PASSBAND)

This design example discusses the suitability of the considered EBG structure for applications requiring better

TABLE 3. Comparison of the −10 dB cutoff frequencies obtained through numerical calculations and EM simulations.

Design Example	ε_{r1}	ε_{r2}	h_1	h_2	w	s	W_P	L_P	f_1 (GHz)				f_2 (GHz)			
			(mm)	(mm)	(mm)	(mm)	(mm)	(mm)	Calc	Sim	Meas	% Error	Calc	Sim	Meas	% Error
1	3	3	0.75	0.19	1.5	1.5	6.5	1.5	8	7.9	-	1.25	12	11.9	-	0.83
2	3.55	3.55	0.508	0.2	1.35	1	3.5	1.5	11.9	12.1	-	1.65	18	19.2	-	6.25
3	2.2	6.15	0.5	0.2	1.35	1	7.5	2.1	6.05	6.3	-	3.9	11.8	12	-	1.6
4	3	3	0.75	0.19	1.6	5	10.1	2	5	5.08	5.16	3.2	7	6.89	7.25	3.5

TABLE 4. Comparison with other modelling techniques.

Ref	Modelling Technique	Purpose	Structure Type	Output	Sample data	% Error
[26]	Circuit Model	Analysis	EBG Structure	circuit values	-	30
[17]	Circuit Model	Analysis	EBG Structure	circuit values	-	-
[38]	ANN	Synthesis	High Pass Filter	circuit values	800	5
[18]	Circuit Model	Analysis	EBG Structure	circuit values	-	4.8
This Work	Curve Fitting	Synthesis	EBG Structure	structure dimensions	126	6.2

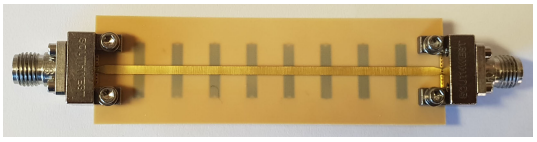

(a)

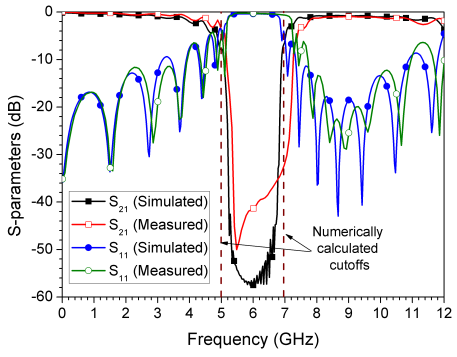

(b)

FIGURE 17. (a) Fabricated filter structure. (b) Simulated and measured S-parameters curves showing the performance of the filter discussed in design example 4.

return loss performance in the passband. As an example, a stopband of 5 to 7 GHz is targeted. For this filter design, the same dielectric materials as discussed in design example 1 are used. In order to achieve better passband performance, lower patch-microstrip interaction is targeted. This is ensured by using a smaller value of patch length L_P and larger value for patch-to-patch spacing s. By using the steps mentioned in Section V, the first-pass approximation is made to get the required frequency cutoffs. The numerically calculated structure dimensions are $W_P = 10.1$ mm, $L_P = 2$ mm, $s = 5$ mm and $w = 1.6$ mm. The fabricated filter structure using the numerically calculated dimensions is shown in Fig. 17(a). Simulated and measured results in Fig. 17(b) confirm that the stopband cutoffs match the numerically calculated values with an improved performance of the return loss and insertion loss in the passband, which is suitable for practical applications.

In order to ascertain the validity of the synthesis method, a comparison for the −10 dB cutoff frequencies of all the test models obtained through numerical calculations and EM simulations are tabulated in Table 3. Absolute percentage error values calculated between the numerical calculations and EM simulations are reported. It can be observed that the maximum error with these design examples remains less than 7%. This shows the validity of the proposed closed form equations and design scheme. Maximum absolute percentage error may be reduced further by including the effect of via radius R_V and height of prepreg in (14) and (15). However, from a designer perspective, such parameters can be better accommodated during later stages such as detailed electromagnetic simulations than in early stages.

A detailed comparison of the proposed method with other modelling techniques is presented in Table 4. The comparison shows the advantage of the proposed method in synthesizing the physical dimensions of the considered EBG structure. The equivalent circuit model presented in [18] offers greater accuracy than the proposed method. However, circuit models approximations are more useful as an analysis tool than a synthesis tool as they offer limited information in determining the physical dimensions of the structure. On the other hand, artificial neural networks (ANN) have advantages as far as accuracy and predictability are concerned, but they usually require a large number of sample data for training/validation purposes. For example, in [38], 800 instances are used to train an ANN for mapping circuit performance to lumped component values which is collected through well-established closed form equations. Implementation of ANN for relatively complex structures would require a fairly large amount of data for training/validation purpose. Since the structure considered for our study is composed of a multilayer stack-up which involves various structural dimensions, training data sample collection based on EM simulation would further aggravate the problem. However, with the help of a comparatively simple curve fitting technique, we have formulated the design procedure for the design of periodic structures having a rectangular patch shorted from both ends. The proposed

scheme based on detailed parametric studies demonstrates first-pass success with at least 94.2% accuracy. The proposed method will lead to a faster design alternative to dispersion analysis and circuit model approximations conventionally used in the initial stages of the design.

VI. CONCLUSION

Physical structure parameters as a function of stop band frequency and bandwidth is developed numerically and then used to create a synthesis methodology for microwave EBG filter structures. A set of closed-form equations are developed from extensive EM analysis to determine the frequency cut-offs offered by this structure based on its physical dimensions. To verify the proposed numerical formulas, two filters were fabricated and measured. Numerical calculations, simulations and measurements show a good agreement with each other. The proposed set of closed-form equations represent the EM simulated data up to an accuracy of 94%. A step-by-step design procedure is devised to help designers quickly calculate the structure physical dimensions from the proposed closed-form equations. This can later be fine-tuned with EM simulations to meet the desired specifications if required. The design scheme is also tested for various sets of patch dimensions and substrate parameters offering stopbands for different frequency bands. The proposed method is able to correctly predict the structure dimensions for desired specifications with a maximum absolute percentage error of 7%. Finally, the proposed design scheme not only provide an accurate estimate of physical dimensions but also saves extensive simulation effort required when tuning these structures.

REFERENCES

[1] F. Martin, *Artificial Transmission Lines for RF and Microwave Applications*. Hoboken, NJ, USA: Wiley, 2015.

[2] M. Chudzik, I. Arnedo, A. Lujambio, I. Arregui, F. Teberio, D. Benito, T. Lopetegi, and M. A. G. Laso, "Design of EBG microstrip directional coupler with high directivity and coupling," in *Proc. 42nd IEEE Eur. Microw. Conf. (EuMC)*, Oct. 2012, pp. 483–486.

[3] M. Zhou, J. Xu, S. D. Luo, and L. J. Xue, "Ka-band fourth harmonic mixer with 1-D EBG structure," *J. Infr. Millim. Waves*, vol. 25, no. 2, pp. 147–149, Apr. 2006.

[4] A. Cismaru, M. Aldrigo, A. Radoi, and M. Dragoman, "Carbon nanotube-based electromagnetic band gap resonator for CH_4 gas detection," *J. Appl. Phys.*, vol. 119, no. 12, Mar. 2016, Art. no. 124504.

[5] S. Jam and M. Simruni, "Performance enhancement of a compact wide-band patch antenna array using EBG structures," *AEU-Int. J. Electron. Commun.*, vol. 89, pp. 42–55, May 2018.

[6] M. K. Abdulhameed, M. S. B. M. Isa, Z. Zakaria, I. M. Ibrahim, M. K. Mohsen, M. L. Attiah, and A. M. Dinar, "Radiation control of microstrip patch antenna by using electromagnetic band gap," *AEU-Int. J. Electron. Commun.*, vol. 110, Oct. 2019, Art. no. 152835.

[7] M. K. Abdulhameed, M. M. Isa, Z. Zakaria, I. M. Ibrahim, and M. K. Mohsin, "Radiation pattern control of microstrip antenna in elevation and azimuth planes using EBG and PIN diode," *Int. J. Electr. Comput. Eng.*, vol. 9, no. 1, pp. 332–340, 2019.

[8] J. P. Shinde and P. N. Shinde, "M-shape electromagnetic-bandgap structures for enhancement in antenna performance," *AEU-Int. J. Electron. Commun.*, vol. 70, no. 6, pp. 842–849, Jun. 2016.

[9] J.-Y. Lee, J. Choi, J.-H. Jang, and W. Hong, "Performance enhancement in compact inverted-L antenna by using 1-D EBG ground structures and beam directors," *IEEE Access*, vol. 7, pp. 93264–93274, 2019.

[10] Y. Guo, S. Kim, H. Gao, and G.-P. Li, "Compact high Q configurable quint-band electromagnetic bandgap filter," *IEEE Access*, vol. 6, pp. 63703–63711, 2018.

[11] I. Arnedo, M. Chudzik, J. M. Percaz, I. Arregui, F. Teberio, D. Benito, T. Lopetegi, and M. A. G. Laso, "Synthesis of one dimensional electromagnetic bandgap structures with fully controlled parameters," *IEEE Trans. Microw. Theory Techn.*, vol. 65, no. 9, pp. 3123–3134, Sep. 2017.

[12] H. Zhu and J. Mao, "Miniaturized tapered EBG structure with wide stopband and flat passband," *IEEE Antennas Wireless Propag. Lett.*, vol. 11, pp. 314–317, 2012.

[13] S. M. S. Hassan, M. N. Mollah, M. A. Rashid, N. H. Ramly, and M. Othman, "Dumbbell shape EBG structure—Worth to EBG assisted microwave filter designing," in *Proc. IEEE Asia–Pacific Conf. Appl. Electromagn. (APACE)*, Dec. 2012, pp. 1–5.

[14] S. M. S. Hassan and M. N. Mollah, "Identical performance from distinct conventional electromagnetic bandgap structures," *IET Microw., Antennas Propag.*, vol. 10, no. 12, pp. 1251–1258, Sep. 2016.

[15] R. S. Kshetrimayum, S. Subramanian Karthikeyan, and D. Dey, "Bandgap determination of triangular lattice EBGs in the ground plane," *AEU-Int. J. Electron. Commun.*, vol. 63, no. 8, pp. 699–702, Aug. 2009.

[16] J. Hester, E. Nguyen, J. Tice, and V. Radisic, "A novel 3D-printing-enabled 'roller coaster' transmission line," in *Proc. IEEE Int. Symp. Antennas Propag. USNC/URSI Nat. Radio Sci. Meeting*, Jul. 2017, pp. 2639–2640.

[17] N. Yang and Z. N. Chen, "Microstrip line periodic structures with capacitive and resonant element loads," in *Proc. IEEE Int. Workshop Antenna Technol., Small Antennas Novel Metamater.*, Mar. 2005, pp. 391–394.

[18] L. Matekovits, D. Thalakotuna, K. P. Esselle, S. G. Hay, and M. Heimlich, "Equivalent-circuit models for efficient transmission and dispersion analyses of multi-state periodic structures," *Prog. Electromagn. Res.*, vol. 153, pp. 93–102, 2015.

[19] I. Shahid, D. N. Thalakotuna, D. K. Karmokar, and M. Heimlich, "Asymmetric transversal patch loaded microstrip line based 1-D periodic structure with flexible selection of stopband resonance," *AEU-Int. J. Electron. Commun.*, vol. 114, Feb. 2020, Art. no. 153010.

[20] L. Matekovits, M. Heimlich, and K. P. Esselle, "Metamaterial-based millimeter-wave switchable leaky wave antennas for on-chip implementation in GaAs technology," *J. Electromagn. Waves Appl.*, vol. 25, no. 1, pp. 49–61, Jan. 2011.

[21] I. Shahid, D. Thalakotuna, and M. Heimlich, "A bi-patch loaded microstrip line based 1-D periodic structure with enhanced stop bandwidth and band switching characteristics," *J. Electromagn. Waves Appl.*, vol. 33, no. 10, pp. 1329–1342, Jul. 2019.

[22] S. M. Sifat, M. M. M. Ali, S. I. Shams, and A.-R. Sebak, "High gain bow-tie slot antenna array loaded with grooves based on printed ridge gap waveguide technology," *IEEE Access*, vol. 7, pp. 36177–36185, 2019.

[23] C.-H. Tsai and T.-L. Wu, "A broadband and miniaturized common-mode filter for gigahertz differential signals based on negative-permittivity metamaterials," *IEEE Trans. Microw. Theory Techn.*, vol. 58, no. 1, pp. 195–202, Jan. 2010.

[24] B.-F. Su and T.-G. Ma, "Miniaturized common-mode filter using coupled synthesized lines and mushroom resonators for high-speed differential signals," *IEEE Microw. Wireless Compon. Lett.*, vol. 25, no. 2, pp. 112–114, Feb. 2015.

[25] A. Fernández-Prieto, J. Naqui, F. Medina, J. Martel, F. Martín, F. Mesa, J. Hong, and S. Qian, "Common-mode suppression for balanced bandpass filters in multilayer liquid crystal polymer technology," *IET Microw., Antennas Propag.*, vol. 9, no. 12, pp. 1249–1253, Sep. 2015.

[26] S. Shahparnia and O. M. Ramahi, "A simple and effective model for electromagnetic bandgap structures embedded in printed circuit boards," *IEEE Microw. Wireless Compon. Lett.*, vol. 15, no. 10, pp. 621–623, Oct. 2005.

[27] H. A. Wheeler, "Transmission-line properties of parallel strips separated by a dielectric sheet," *IEEE Trans. Microw. Theory Techn.*, vol. 13, no. 2, pp. 172–185, Mar. 1965.

[28] E. Hammerstad and O. Jensen, "Accurate models for microstrip computer-aided design," in *IEEE MTT-S Int. Microw. Symp. Dig.*, May 1980, pp. 407–409.

[29] D. N. P. Thalakotuna, K. P. Esselle, L. Matekovits, M. Heimlich, and S. G. Hay, "Changing the electromagnetic bandgap and stopbands in a multistate periodic circuit," *Microw. Opt. Technol. Lett.*, vol. 55, no. 8, pp. 1871–1874, Aug. 2013.

[30] L. Matekovits, M. Bercigli, and R. Guidi, "Efficient electromagnetic characterization of a 1D reconfigurable periodic configuration in microstrip technology," in *Proc. Int. Conf. Electromagn. Adv. Appl. (ICEAA)*, Sep. 2012, pp. 167–169.

[31] Z. Ning Chen, N. Yang, Y. Yi Wang, and M. Y. W. Chial, "A novel compact electromagnetic bandgap (embg) structure and its application for antenna duplexer," in *Proc. IEEE Radio Wireless Conf. (RAWCON)*, Aug. 2002, pp. 71–74.
[32] L.-J. Zhang, C.-H. Liang, L. Liang, and L. Chen, "A novel design approach for dual-band electromagnetic band-gap structure," *Prog. Electromagn. Res.*, vol. 4, pp. 81–91, 2008.
[33] Y. Kusama and R. Isozaki, "Compact and broadband microstrip bandstop filters with single rectangular stubs," *Appl. Sci.*, vol. 9, no. 2, p. 248, Jan. 2019.
[34] M. Abdelfattah, M. Hickle, M. D. Sinanis, Y.-C. Wu, and D. Peroulis, "A 12–20 GHz passively-compensated tunable bandstop filter with 40-dB notch level," in *IEEE MTT-S Int. Microw. Symp. Dig.*, Jun. 2018, pp. 571–574.
[35] S. Song, S. X. Chew, X. Yi, L. Nguyen, and R. A. Minasian, "Tunable single-passband microwave photonic filter based on integrated optical double notch filter," *J. Lightw. Technol.*, vol. 36, no. 19, pp. 4557–4564, Oct. 1, 2018.
[36] L. Matekovits, M. Heimlich, and K. P. Esselle, "Tunable periodic microstrip structure on GaAs wafer," *Prog. Electromagn. Res.*, vol. 97, pp. 1–10, 2009.
[37] L. Yang, M. Fan, F. Chen, J. She, and Z. Feng, "A novel compact electromagnetic-bandgap (EBG) structure and its applications for microwave circuits," *IEEE Trans. Microw. Theory Techn.*, vol. 53, no. 1, pp. 183–190, Jan. 2005.
[38] A. Ilumoka and J. Gaudiana, "Neural network-based tunable microwave filter design for re-configurable biomedical hardware," in *IEEE MTT-S Int. Microw. Symp. Dig.*, Dec. 2014, pp. 1–3.
[39] D. Nesic and A. Nesic, "Bandstop microstrip PBG filter with sinusoidal variation of the characteristic impedance and without etching in the ground plane," *Microw. Opt. Technol. Lett.*, vol. 29, no. 6, pp. 418–420, 2001.
[40] C.-S. Kim, J.-S. Park, D. Ahn, and J.-B. Lim, "A novel 1-D periodic defected ground structure for planar circuits," *IEEE Microw. Guided Wave Lett.*, vol. 10, no. 4, pp. 131–133, Apr. 2000.
[41] S. Ying Huang and Y. Hui Lee, "Tapered dual-plane compact electromagnetic bandgap microstrip filter structures," *IEEE Trans. Microw. Theory Techn.*, vol. 53, no. 9, pp. 2656–2664, Sep. 2005.

IRFAN SHAHID (Student Member, IEEE) received the B.E. degree in avionics engineering from the National University of Sciences and Technology (NUST), Pakistan, in 2005, and the M.S. degree in computer science and technology from the University of Electronic Science and Technology of China (UESTC), Chengdu, China, in 2013. He is currently pursuing the Ph.D. degree with the Faculty of Science and Engineering, Macquarie University, Australia. His current research interests include electromagnetic bandgap structures, reconfigurable circuits, impedance transformers, and circuits for microwave applications.

DUSHMANTHA N. THALAKOTUNA (Senior Member, IEEE) received the B.Sc. degree in electronics and telecommunication from the University of Moratuwa, Sri Lanka, in 2008, and the Ph.D. degree in electronic engineering from Macquarie University, Australia, in 2012. He has worked as a Radio Frequency Engineer and a Systems Engineer in commercial and defence sector for over seven years. He is currently a Lecturer with the School of Electrical and Data Engineering, University of Technology Sydney, Australia. His current research interests include MMICs, Satcom antennas, base station antennas, reconfigurable microwave and millimeter wave circuits, and periodic structures.

DEBABRATA K. KARMOKAR (Senior Member, IEEE) received the B.Sc. degree in electrical and electronic engineering (EEE) from the Khulna University of Engineering & Technology (KUET), Khulna, Bangladesh, in 2007, and the Ph.D. degree in electronic engineering from Macquarie University, Sydney, NSW, Australia, in 2015.

He joined KUET, as a Lecturer, in 2007, where he was promoted to an Assistant Professor, and also served as an Assistant Director of Students' Welfare of the university. From 2012 to 2015, he was a Casual Academic, a Research Assistant, and a Secretary of the IEEE Student Branch, Macquarie University. From 2016 to 2019, he was a Postdoctoral Research Associate with the Global Big Data Technologies Centre (GBDTC), University of Technology Sydney (UTS), Australia. From 2019 to 2020, he was a Lecturer with the School of Engineering, Macquarie University. He is currently a Lecturer with the UniSA STEM, University of South Australia, Mawsoon Lake, SA, Australia.

Dr. Karmokar was a recipient of several scholarships and awards, including the Young Scientist Award from Venus International Foundation, in 2018, and the URSI Young Scientist Award, in 2019. He is serving as a Reviewer for several journals for the IEEE, IET, Wiley, MDPI, Hindawi, Taylor & Francis, Springer, and Elsevier. He is also serving as an Associate Editor for IEEE ACCESS.

MICHAEL HEIMLICH (Senior Member, IEEE) received the B.S. (magna cum laude), M.E., and Ph.D. degrees from the Rensselaer Polytechnic Institute, Troy, NY, USA. He joined Macquarie University, Sydney, in 2009, after 25 years in industry, where he is currently a Professor with the School of Engineering. His current research interests include mm-wave reconfigurable electronics and formal methods in RF/microwave design.